Macromolecules
NOTE

Macromolecules **2009**, *42*, 5895–5899 **5895**
DOI: 10.1021/ma9006335

Directed Self-Assembly of Lamellar Microdomains of Block Copolymers Using Topographic Guiding Patterns

Sang-Min Park, Charles T. Rettner, Jed W. Pitera, and Ho-Cheol Kim*

IBM Almaden Research Center, 650 Harry Road, San Jose, California 95120

Received March 24, 2009; Revised Manuscript Received June 23, 2009

Introduction

Thin films of block copolymers are of great interest for their practical applications in surface patterning, since they offer a potential low-cost option for extending the length scales of features below that achievable with optical lithography.[1−5] Despite more than a decade of study, much remains to be learned about the best approach to obtaining patterns with low-dimensional variation and defectivity. In general, for practical block copolymer nanofabrication, three key parameters must be controlled: orientation of microdomains with respect to the substrate, lateral alignment on the substrate, and registration to guiding features. The placement of microdomains has so far been controlled by prepatterning the substrate with either topographical guiding patterns (graphoepitaxy)[6−9] or surface chemical patterns (chemical epitaxy).[10−13] The latter approach gives precise placement control when the length scales of the chemical patterns match with those of microdomains of the block copolymer. The placement of lamellae following the layouts of line patterns with various geometries used in electronic devices has also been demonstrated.[14] More recently, it has been shown that microdomains can be aligned using sparse chemical patterns with a pitch several times greater than that of the domains.[15,16] Graphoepitaxy has also been successfully employed to direct the self-assembly of microdomains. Typically a pair of ridges is prepared by lithography, and the surface energy of the sidewalls and bottom is carefully controlled before coating with the block copolymer film. When the sidewalls have a selective interaction with one phase of the block copolymer and the bottom surface is nonselective, lamellar microdomains are found to align parallel to the sidewalls, thus subdividing the distance between the ridges.[9,17,18] The alignment of lamellae perpendicular to the sidewalls has also been demonstrated, by tuning the surface energy of both the sidewalls and the bottom surface to be nonselective.[19] The latter approach removes the undesirable reflection of sidewall roughness in the line edge roughness of the lamellae, which is a major drawback of the parallel alignment strategy. Besides lamellar microdomain, cylinder-forming block copolymers have been employed to generate the alignment both parallel and perpendicular to the sidewall.[20,21] Sundrani and coworkers reported that thermal flow and confinement of polymer drives perpendicular orientation of cylindrical microdomains within topographic guiding patterns.[21]

However, this perpendicular alignment is energetically invariant to translation of the microdomains parallel to the ridges, so it is difficult to precisely register the microdomains relative to the guiding patterns. In this study, we report an extension of the graphoepitaxy approach, in which we have obtained precise registration of lamellar microdomains of poly(styrene-*b*-methyl methacrylate) (PS-*b*-PMMA) contained in a trench formed between two raised bars, as shown schematically in Figure 1. The key to the registration of the position of the microdomains along the trench is the sharp step placed at the end of the ridges. This two-level topographic guiding pattern thus provides simultaneous alignment and registration of lamellar microdomains. We have used a strategy of combined experiment and simulation to better understand the registration mechanism.

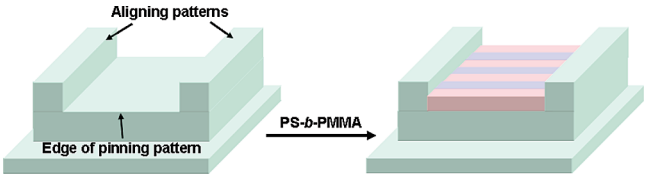

Figure 1. Schematic representation of the placement control of lamellar microdomains in this study. Two levels of topographical guiding patterns are used to achieve both alignment and registration of lamellar microdomains.

Experimental Section

Sample Preparation. The patterned substrates were fabricated by first coating a SiO_2 substrate with 100 nm of polyimide and then depositing 20 nm of titanium (Ti) on the polyimide. Subsequently, a 50 nm thick hydrogen silsesquioxane (HSQ) layer was deposited as a negative photoresist on the Ti layer. Line structures with 200, 300, and 400 nm widths were then created on the HSQ surface by electron beam lithography.[19] After developing in 0.26 N tetramethylammonium hydroxide developer, this negative resist consisted of an HSQ inorganic polymer with $HSiO_{3/2}$ repeat units. The resist itself, therefore, forms the ridge structures. In order to create the sharp step to interrupt the lamellar microdomains, we next carried out a second level of lithography using a positive resist (KRS). This resist was patterned with e-beam lithography to form openings across the HSQ resist lines. Using the KRS as a mask, we then etched the Ti layer with a CF_4 etch sufficient to cut completely through the Ti. We then etched the polyimide with O_2 gas to remove the layer and form a 100 nm step in the polyimide. With this approach, we could also etch under the Ti to produce a ~100 nm undercut under the Ti, which is not affected by the O_2 etch. During the O_2 plasma, the KRS layer was also stripped, and the pattern surface was simultaneously oxidized. A thin layer of hydroxyl-terminated random copolymer of styrene and methyl methacrylate (PS-*r*-PMMA) was spin-coated onto the patterned substrates from a 1 wt % toluene solution and then annealed at 200 °C for 2 h under a nitrogen environment to anchor the PS-*r*-PMMA brush. Ungrafted PS-*r*-PMMA was washed away by repeated rinsing with toluene. Symmetric PS-*b*-PMMA (M_n = 36 kg/mol) purchased from Polymer Source, Inc., was

*To whom correspondence should be addressed: e-mail hckim@us.ibm.com; Tel 408-927-3725; Fax 408-927-3310.

Published on Web 07/06/2009

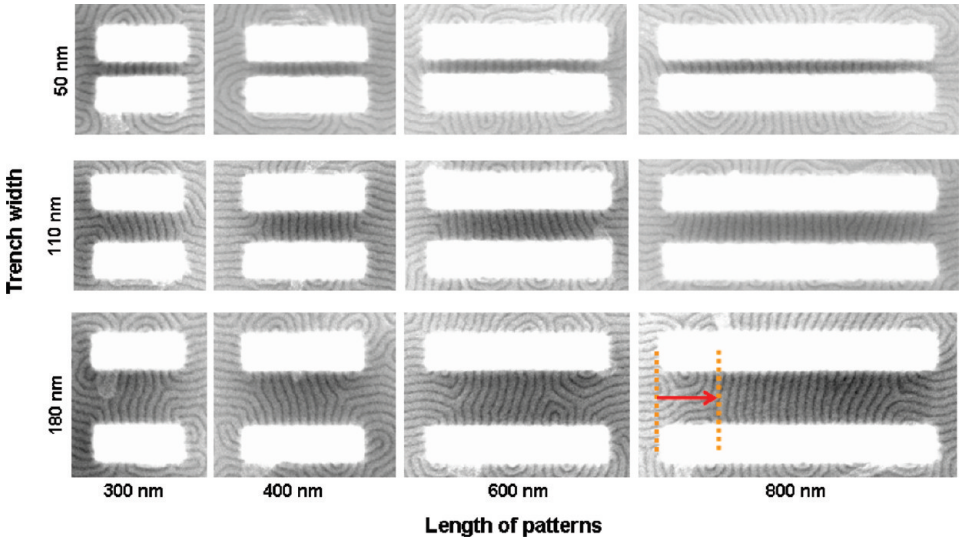

Figure 2. Plan-view SEM micrographs of the lamellar microdomains confined between two parallel ridges. The lamellar microdomains align perpendicular to the side walls of the guding ridges.

spin-coated from 1 wt % toluene solution onto the neutral brush grafted substrates and subsequently annealed at 190 °C for 5 h under a nitrogen environment. The film thickness evaluated using a NanoSpec/AFT 4150 (Nanometrics Inc.) was about 30 nm on a flat region. The resulting morphology was imaged without any metal deposition using a LEO 1550-VP field emission scanning electron microscope (FE-SEM) with a 1 kV acceleration voltage.

Single Chain in Mean-Field (SCMF) Monte Carlo Simulation. Simulations were carried out on symmetric 16-mer bead−spring block copolymer chains (reduced bond force constant 1.0, bond length 3.0, $\chi = 1.0$, and $\kappa = 25$) using a lattice spacing of $R_g/4.5$. With these parameters, the lamellar period (L_0) of this polymer is ~18 lattice units. In lattice units, the simulation domain was 400 units long by 300 wide, with a uniform film thickness of 16 units, and was periodic only across its width. 2.64×10^6 chains (42.24×10^6 interaction sites) were simulated, producing a density of 21 sites/lattice element. Simulations were started in a disordered melt and carried out for 5000 Monte Carlo sweeps, with 10 moves/site/sweep. The mean-field site densities were updated every Monte Carlo sweep. To model the experimental geometry, the step edge was introduced by raising one-half of the simulation domain 48 units above the lower half. Simulations were repeated with the film thickness along the resulting vertical face set at 0, 6, 8, or 16 lattice units. Two raised pads ($105 \times 8 \times 16$ lattice units) on the upper half separated by a gap of either 40 or 60 lattice units model the guiding patterns on the upper topography. There are some limitations of the system geometry used in the simulations. First, the lack of periodicity along the long axis of the simulation volume (i.e., perpendicular to the pinning edge) creates hard neutral walls that bound both the upper and lower films. These hard walls induce nematic order in the lamellar block copolymer, causing a strong preference for the simulated lamella to orient parallel to the long axis (and perpendicular to the pinning edge). Second, the neutral vapor interface can induce a similar nematic orientation in the upper film at the pinning edge. A schematic comparing the simulation and experimental geometries is included in the Supporting Information.

In the main set of simulations, both the substrate and vapor surfaces were treated as energetically neutral for the block copolymer. As a result, the simulations show no preference for the half-lamella at the edge of the pinning pattern to be formed from PS or PMMA. This neutral interface also means that outside the guiding pattern lamella of the upper film tend to orient perpendicular to the edge of the pinning pattern since there is no differential surface tension to counteract the nematic force arising from the "wall" of the vapor interface. A second set of exploratory calculations were also performed where the vapor interface at the edge of the pinning pattern was selective for the simulated PS block (reflecting the lower surface tension of PS versus PMMA). With this more realistic vapor interface, the half-lamella was always formed by the PS block in simulations, suggesting that a similar preference may occur experimentally. In addition, simulations with the more realistic differential surface tension also yielded lamella oriented parallel to the pinning edge both inside and outside the guiding patterns, as seen in experiment. Images of the differential surface tension calculations showing both consistent registration of a PS half-domain at the pinning edge as well as this bulk parallel orientation in the upper film are included in the Supporting Information.

Results and Discussion

The pair of parallel ridges (or bars), hereafter denoted as the *aligning patterns*, guide the alignment of the lamellae perpendicular to the sidewalls, as mentioned above. The sharp step at the end of the aligning patterns, hereafter denoted as the *pinning pattern* or *mesa*, is oriented perpendicular to the longitudinal direction of the aligning patterns, as shown in Figure 1. The surface of all the topographic patterns is modified to be nonselective to both PS and PMMA by anchoring a random copolymer of PS and PMMA. Subsequent spin-coating of a PS-*b*-PMMA solution followed by thermal annealing yields arrays of lamellae with controlled alignment and registration.

Figure 2 shows plan-view SEM micrographs of lamellae confined in the aligning patterns without pinning patterns. PS-*b*-PMMA (M_n = 36 kg mol^{-1}) is confined within the aligning patterns with various width (50−180 nm) and length (300−800 nm) while the height is maintained as ~50 nm. The surface of both the bottom and sidewall was covered by a brush layer of PS-*r*-PMMA with 58 vol % of PS.[23] A toluene solution of PS-*b*-PMMA was spun-cast to generate thin films of the block copolymer. The thickness of the PS-*b*-PMMA was ~30 nm on the flat region of the substrate. Samples were subsequently annealed at 190 °C for 5 h under nitrogen environment. As shown in the SEM images in Figure 2, the nonselective nature of bottom surface orients the lamellar microdomains perpendicular to the surface; hence, the plan-view images show line patterns from lamellar microdomains. It is clear that the aligning patterns,

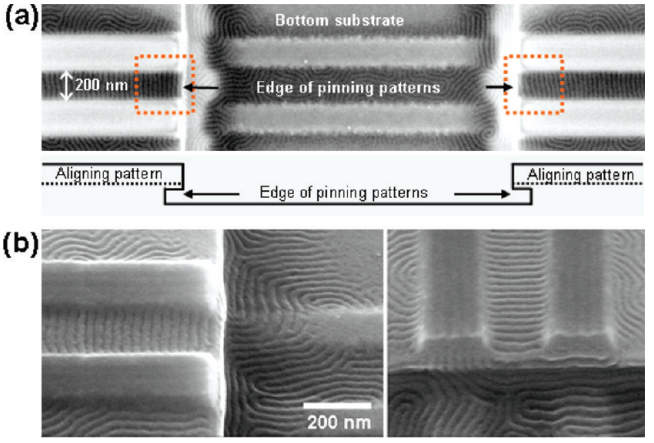

Figure 3. (a) Plan-view and (b) tilted-view of SEM micrographs of the lamellar microdomains assembled on the two levels of topographic guiding patterns. The scheme shown at the bottom of (a) represents a cross-sectional profile. Images from two different angles of tilting are shown in (b).

which are shown as thick white stripes, render the alignment of lamellae perpendicular to the sidewalls. This behavior is also due to the nonselective property of the sidewall surface, which also favors a perpendicular orientation. The gap between the aligning patterns also affects the density of defects in the lamellae. As we reported in our previous work, the defect density increases with the gap between topographical guiding patterns.[19] When the gap is much larger than the orientational correlation length of lamellar microdomains, only localized alignment of lamellae is observed near the sidewalls of aligning patterns. It is also clear that the alignment of lamellae has more defects at the end of the aligning patterns. This behavior is most likely due to the influence of the random alignment of lamellae outside of the aligning patterns. The lamellae between the aligning patterns form a single "grain", which then necessarily forms grain boundaries (and defects) with the randomly oriented lamellar domains outside the aligning patterns. The defective alignment at the end of the aligning patterns becomes more significant as the gap between the aligning patterns increases.[24]

The effect of pinning patterns on the registration of lamellae is shown in a plan-view SEM image in Figure 3a. It is clear that the edge of the pinning pattern (or "mesa") effectively locates one phase of the lamellar microdomains. Though it is unclear to determine which phase is located at the edge of the pinning pattern from the experimental data, the simulation result that will be discussed below suggests that PS phase preferentially locates at the edge due to lower surface energy. A SEM micrograph from a different angle reveals the precise pinning of lamellae at the edge of the mesa, as shown in Figure 3b. It was observed that the pinning of microdomains becomes less regular with increasing thickness of block copolymer film on the side wall of pinning pattern (mesa). An undercut was introduced to the side wall of the mesa (shown schematically at the bottom of Figure 3a) to control the meniscus and thus to control the film thickness at the side wall of the mesa (see Supporting Information and Figures S1 and S2 for more details on the substrate preparation).

A plan-view SEM micrograph in Figure 4a shows that good alignment of lamellae is obtained with the aligning patterns with gaps up to 300 nm, while very defective alignment is obtained with 400 nm gap patterns (Figure 4c). It is interesting to note that the lamellae in Figure 4a align almost perfectly up to 300 nm gap while many defects are observed in the aligning patterns of 180 nm in gap shown in Figure 2. This is likely due to the pinning of PS domain, which has lower surface tension, at the air/pinning pattern interface. Hence, the pinning pattern provides an

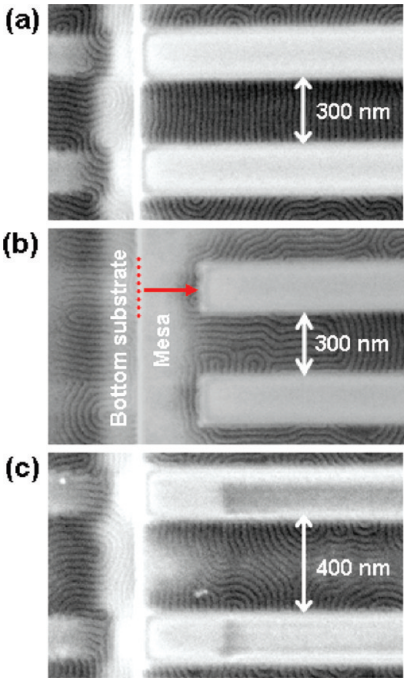

Figure 4. Plan-view SEM micrographs of the lamellar microdomains assembled on the two levels of topographical guiding patterns: (a) guiding pattern of 300 nm in width; (b) guiding pattern of 300 nm in width mismatched with pinning pattern; (c) guiding pattern of 400 nm in width. The area marked as "bottom substrate" is recessed from the "mesa" area.

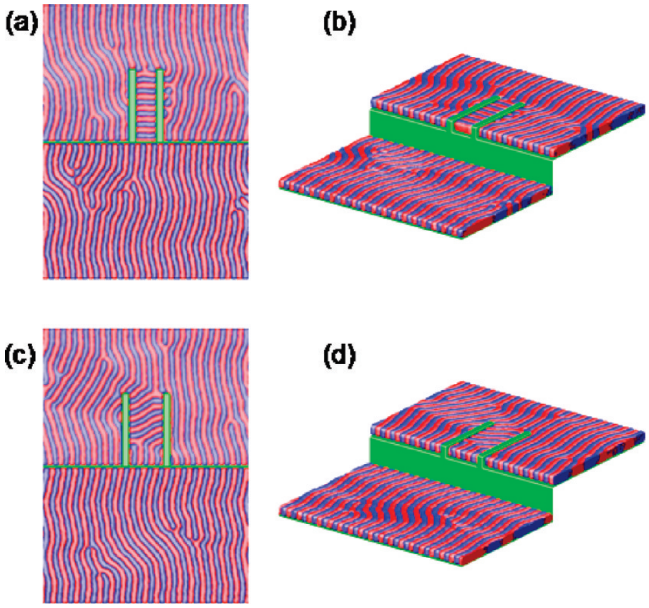

Figure 5. Top (a, c) and tilted (b,d) views of SCMF Monte Carlo simulations of lamellae-forming block copolymer thin films on a substrate similar to the experiment. The interpad spacing of guiding patterns is (a, b) 40 and (c, d) 60 lattice units, and the film thickness of the vertical surface is 0.

additional constraint, which enhances the alignment of lamellae along the edge of the pinning pattern. Figure 4b re-emphasizes the effect of the edge on pinning lamellar microdomains. We used an intentionally mismatched edge of the pinning pattern with the guiding patterns. The alignment of lamellae is very defective in this micrograph, similar to the alignment characteristics shown in Figure 2. This result clearly indicates that the edge of pinning

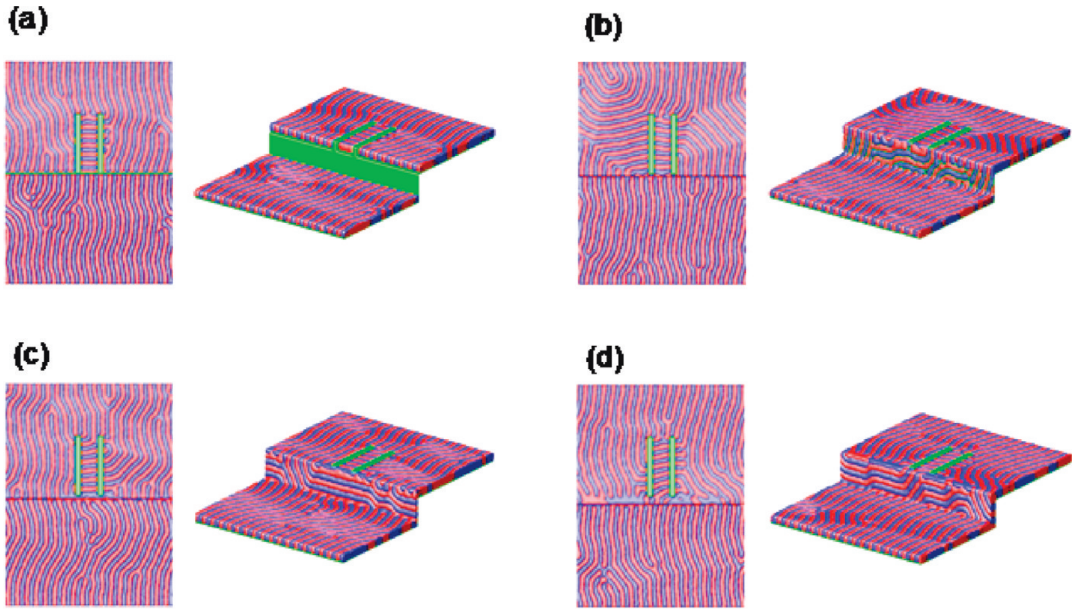

Figure 6. Simulation results of lamellar phase block copolymer films with varying thickness along the vertical surface of pinning pattern. The thickness of vertical surface is (a) 0, (b) 6, (c) 8, and (d) 16 lattice units.

pattern plays a crucial role in the alignment and registration of the lamellar microdomains.

To provide additional structural insights into the influence of the substrate geometry, we also simulated a thin film of an idealized symmetric block copolymer in the presence of model substrate topographies that included both the guiding and pinning patterns. These simulations were carried out using our distributed memory parallel implementation of single chain in mean-field Monte Carlo[25] on an IBM BlueGene/L[26] system and visualized using OpenDX.[27] The single chain in mean-field Monte Carlo model allows the efficient, highly parallel simulation of bulk and thin film polymer melts by replacing nonbonded segment−segment interactions with a segment-density mean-field approximation.[28]

A symmetric block copolymer thin film was simulated atop a neutral substrate with varying geometries of aligning and pinning patterns. The simulation results broadly support the experimental observations. Figure 5 shows top and tilted views of the simulation results for the substrate with interpad spacing of aligning patterns 40 and 60 lattice unit (L_0 is ~18 units) while the film thickness along the vertical face (side wall of pinning pattern) was kept at 0. Consistent with experimental data shown in Figures 3 and 4, perpendicular alignment between the aligning ridges could be improved by decreasing the simulated interpad spacing. Because the entire substrate is energetically nonselective, the vertical edge of the mesa also induces a perpendicular orientation of the lamella at the lower substrate surface. With a nonzero film thickness on the vertical surface, this orientation can propagate up along the vertical film to interfere with the block copolymer on the top surface. Our simulations also show that a selective vapor interface can consistently drive the half-lamella at the edge of the pinning pattern to be formed from the block with lower surface tension (PS). The selective vapor interface also produces a more realistic parallel orientation (parallel to the pinning edge) for lamellae in the upper film outside of the guiding pattern.

It is worth noting that the simulation geometry does not exactly match the experimental one and tends to induce a significant and unphysical orientation of lamellar domains perpendicular to the pinning edge in both the upper and lower films. This is due to the additional hard walls constraining the simulated films. This unphysical bulk perpendicular orientation can certainly interfere with the observed parallel orientation of the lamellae between the aligning pads. It also interferes with the experimentally observed tendency for lamellae to orient perpendicular to the exterior walls of the aligning pads, which is only seen in a few of our simulations. This interference is not present in the experiment, where the orientation of the lamellae far from the pinning and guiding patterns is uncontrolled. As a result, we expect that our simulations underestimate the robustness of parallel alignment and registration. We have also monitored the process of self-assembly over the course of each Monte Carlo simulation and consistently observe formation of the parallel lamellar structures in the channel before the bulk perpendicular orientation has coarsened significantly.

The effect of film thickness along the vertical face of pinning pattern is shown in Figure 6. The interpad spacing of the aligning patterns was fixed at 40 lattice units. Increasing film thickness along the vertical face from 0 to 6, 8, or 16 lattice units roughly corresponds to increasing the meniscus. When there is significant film thickness along the vertical face, perpendicular ordering of the lamellae normal to that face interferes with the ordering between the aligning patterns, as shown in Figure 6d. As mentioned above, the film thickness along the vertical face of the mesa is crucial for pinning of one phase of the microdomains at the edge. Experimentally, this can be achieved by controlling the meniscus using an undercut at the side wall of pinning pattern as shown above or increasing the height of the pinning pattern beyond the capillary wetting height to discontinue the block copolymer films at the edge of the pinning pattern.

In summary, we have demonstrated the combined alignment and registration of lamellar microdomains of PS-*b*-PMMA using two levels of topographical guiding patterns. Experimental results indicate the critical role of the pinning pattern for the alignment and registration. Our simulations suggest that the film thickness at the vertical face of the guiding patterns is a key control parameter for ordered structures and that the differential surface tension of the two blocks provides an energetic mechanism for precise registration of the lamellae.

Acknowledgment. S.-M.P. thanks JSR Micro Co. for their support.

Supporting Information Available: Description of fabrication of topographic prepattern as well as figures illustrating the

simulation geometry, order formation during the course of a simulation, and effect of a PS-selective vapor interface on the simulation results. This material is available free of charge via the Internet at http://pubs.acs.org.

References and Notes

(1) Hawker, C. J.; Russell, T. P. *MRS Bull.* **2005**, *30*, 952.
(2) Segalman, R. A. *Mater. Sci. Eng., R* **2005**, *48*, 191.
(3) Black, C. T.; Ruiz, R.; Breyta, G.; Cheng, J. Y.; Colburn, M. E.; Guarini, K. W.; Kim, H. C.; Zhang, Y. *IBM J. Res. Dev.* **2007**, *51*, 605.
(4) Kim, H. C.; Hinsberg, W. D. *J. Vac. Sci. Technol. A* **2008**, *26*, 1369.
(5) Darling, S. B. *Prog. Polym. Sci.* **2007**, *32*, 1152.
(6) Segalman, R. A.; Yokoyama, H.; Kramer, E. J. *Adv. Mater.* **2001**, *13*, 1152.
(7) Sundrani, D.; Darling, S. B.; Sibener, S. J. *Nano Lett.* **2004**, *4*, 273–276.
(8) Cheng, J. Y.; Ross, C. A.; Smith, H. I.; Thomas, E. L. *Adv. Mater.* **2006**, *18*, 2505.
(9) Park, S. M.; Stoykovich, M. P.; Ruiz, R.; Zhang, Y.; Black, C. T.; Nealey, P. E. *Adv. Mater.* **2007**, *19*, 607.
(10) Rockford, L.; Liu, Y.; Mansky, P.; Russell, T. P.; Yoon, M.; Mochrie, S. G. J. *Phys. Rev. Lett.* **1999**, *82*, 2602.
(11) Kim, S. O.; Solak, H. H.; Stoykovich, M. P.; Ferrier, N. J.; de Pablo, J. J.; Nealey, P. F. *Nature* (*London*) **2003**, *424*, 411.
(12) Stoykovich, M. P.; Muller, M.; Kim, S. O.; Solak, H. H.; Edwards, E. W.; de Pablo, J. J.; Nealey, P. F. *Science* **2005**, *308*, 1442.
(13) Park, S. M.; Craig, G. S. W.; La, Y. H.; Solak, H. H.; Nealey, P. F. *Macromolecules* **2007**, *40*, 5084.
(14) Stoykovich, M. P.; Kang, H.; Daoulas, K. C.; Liu, G.; Liu, C. C.; de Pablo, J. J.; Mueller, M.; Nealey, P. F. *ACS Nano* **2007**, *1*, 168.
(15) Cheng, J. Y.; Rettner, C. T.; Sanders, D. P.; Kim, H. C.; Hinsberg, W. D. *Adv. Mater.* **2008**, *20*, 3155.
(16) Ruiz, R.; Kang, H. M.; Detcheverry, F. A.; Dobisz, E.; Kercher, D. S.; Albrecht, T. R.; de Pablo, J. J.; Nealey, P. F. *Science* **2008**, *321*, 936.
(17) Cheng, J. Y.; Pitera, J.; Park, O. H.; Flickner, M.; Ruiz, R.; Black, C. T.; Kim, H. C. *Appl. Phys. Lett.* **2007**, *91*, 143160.
(18) Ruiz, R.; Ruiz, N.; Zhang, Y.; Sandstrom, R. L.; Black, C. T. *Adv. Mater.* **2007**, *19*, 2157.
(19) Park, S. M.; Park, O. H.; Cheng, J. Y.; Rettner, C. T.; Kim, H. C. *Nanotechnology* **2008**, *19*, 455304.
(20) Sundrani, D.; Darling, S. B.; Sibener, S. J. *Langmuir* **2004**, *20*, 5091.
(21) Sundrani, D.; Sibener, S. J. *Macromolecules* **2002**, *35*, 8531.
(22) Namatsu, H.; Takahashi, Y.; Yamazaki, K.; Yamaguchi, T.; Nagase, M.; Kurihara, K. *J. Vac. Sci. Technol. B* **1998**, *16*, 69.
(23) Mansky, P.; Liu, Y.; Huang, E.; Russell, T. P.; Hawker, C. J. *Science* **1997**, *275*, 1458.
(24) de Gennes, P. G.; Prost, J. *The Physics of Liquid Crystals*, 2nd ed., Oxford University Press: New York, 1993.
(25) Müller, M.; Smith, G. D. *J. Polym. Sci., Part B: Polym. Phys.* **2005**, *43*, 934.
(26) Gara, A.; Blumrich, M. A.; Chen, D.; Chiu, G. L. T.; Coteus, P.; Giampapa, M. E.; Haring, R. A.; Heidelberger, P.; Hoenicke, D.; Kopcsay, G. V.; Liebsch, T. A.; Ohmacht, M.; Steinmacher-Burow, B. D.; Takken, T.; Vranas, P. *IBM J. Res. Dev.* **2005**, *49*, 195.
(27) Open Visualization Data Explorer, v4.4.4 (http://www.opendx.org).
(28) Daoulas, K. Ch.; Müller, M. *J. Chem. Phys.* **2006**, *125*, 184904.